LETTER TO THE EDITOR

Ultrafast multiphoton forest fires and fractals in clusters and dielectrics

L N Gaier[1]**, M Lein**[2]**, M I Stockman**[3]**, P L Knight**[1]**, P B Corkum**[4]**, M Yu Ivanov**[4] **and G L Yudin**[4]

[1] QOLS, Blackett Laboratory, Imperial College London, Prince Consort Road, London SW7 2BW, UK
[2] Max Planck Institute for the Physics of Complex Systems, Nöthnitzer Str. 38, 01187 Dresden, Germany
[3] Department of Physics and Astronomy, Georgia State University, Atlanta, Georgia 30303, USA
[4] National Research Council of Canada, 100 Sussex Drive, Ottawa, Ontario, K1A 0R6, Canada

E-mail: lucien.gaier@imperial.ac.uk, gennady.yudin@nrc.ca, misha.ivanov@nrc.ca and mstockman@gsu.edu

Abstract
We describe the interaction of ultrashort infrared laser pulses with clusters and dielectrics. Rapid ionization occurs on a sub-laser wavelength scale below the conventional breakdown threshold. It starts with the formation of nano-droplets of plasma which grow like forest fires, without any need for heating of the electrons promoted to the conduction band. The dimensionality of the damaged area can be fractal and changes during the laser pulse. This mechanism is operative in both rare gas clusters and dielectrics interacting with ultrashort, moderately intense laser pulses which include only several periods of the driving field, so that the traditional avalanche mechanisms have no time to develop.

Traditionally, dynamics of laser-induced breakdown is divided into several stages. First, conventional multiphoton ionization provides seed population of free electrons. Second, these electrons increase their kinetic energy due to inverse bremsstrahlung in the laser field, as a result of multiple laser-assisted collisions with the lattice. Third, when the electron energy exceeds the band gap, it can collisionally promote the next electron into the conduction band. Clearly, this picture should change when one is dealing with extremely short—few cycles long—and moderately intense low-frequency laser pulses: at some point, the pulse duration should become too short to enable significant heating of the electrons in the conduction band. Where this boundary lies depends on the laser wavelength, intensity, band gap, etc.

Experimentally, permanent modification of refractive index in dielectric materials, such as fused silica (band gap $\sim$9 eV) irradiated by infrared laser pulses (e.g., $\lambda = 800$ nm) and the duration of 30–50 fs occurs at rather moderate intensities about $I \sim 10^{13}$ W cm^{-2} [1, 3 and references therein]. Energies in the pulse sufficient to change the refractive index by $\Delta n \sim (3$–$5) \times 10^{-3}$ are only 50–100 nJ [1, 3]. Thus, permanent modification occurs below the self-focusing and the breakdown thresholds [1]. At these intensities the characteristic electron oscillation energy $U_p = e^2 E^2/4m\omega^2$ ($\omega = 1.57$ eV for $\lambda = 800$ nm is the laser frequency and E is electric field strength) is small, $U_p \simeq 0.6$ eV. Since the energy absorbed by an electron during a collision in the laser field is $\sim U_p$, it is too low to ensure sufficient heating of the electrons in the conduction band to start an electron avalanche within the $\sim$20 fs available after the electron transition to the conduction band. Therefore, a different physical mechanism (or mechanisms) should be responsible for the damage.

Note that very large clusters of rare gas atoms are similar to dielectrics for very short laser pulses, as long as the expansion of the clusters due to ionization is negligible during the pulse. Mechanisms of damage in a dielectric are then similar to mechanisms of ultrafast ionization in a cluster with frozen nuclei. Such mechanisms act at the very early stage of cluster ionization and are complimentary to the ionization and energy absorption mechanisms induced by the cluster expansion [6–8].

We concentrate on one such damage mechanism which becomes operative when the laser pulses are too short (and the intensities and/or energies too low) to induce the traditional avalanche. Mathematically, this damage mechanism can be described as the propagation of forest fires. The core physical effect responsible for laser-induced 'forest fires' in clusters and dielectrics is known as 'enhanced ionization' in molecules [9] and 'ionization ignition' in clusters [10–14]. When electrons localize on the nuclei (e.g., during dissociation of a molecule, or in a rare gas cluster), fast removal of such an electron leaves an uncompensated positive charge behind—a hole. In the tunnelling regime of $I_p \ll U_p$, where I_p is the ionization potential of an atom in a cluster, the quasi-static tunnelling rate (we use atomic units throughout the paper unless otherwise specified)

$$\Gamma_{qs}(t) \propto \exp\left(-\frac{2(2I_p)^{3/2}}{3|\mathbf{E}_0 \cos \omega t|}\right) \tag{1}$$

is exponentially modified by adding the electric field of the hole $\mathbf{E}_h$ to the electric field of the laser $\mathbf{E}(t) = \mathbf{E}_0 \cos \omega_t$: $|\mathbf{E}_0 \cos \omega t| \rightarrow |\mathbf{E} \cos \omega t + \mathbf{E}_h|$ [9, 10]. Thus, creation of a hole exponentially enhances creation of new holes at the adjacent sites. New holes continue the same trend [15], igniting an avalanche-like ionization in a cluster or in a molecule [9, 10].

Here, we describe ultrafast dynamics of the development of this damage mechanism and show that it creates nano-scale droplets of singly ionized plasma. We show that these nano-structures expand similar to forest fires and can have fractal dimension. We further suggest that in dielectrics this damage mechanism is capable of creating permanent nano-scale modification of refractive index with the size of modified areas much smaller than the laser wavelength.

Compared to the standard ionization ignition dynamics in clusters [10–14], the main qualitative differences of the 'forest fire' dynamics described here are two fold. Firstly, we focus on the moderate range of intensities and intermediate values of the Keldysh parameter [16] $\gamma = \sqrt{I_p/2U_p} \geqslant 1$. Secondly, we consider extended medium and neglect any effects coming from the physical boundaries of the system. Physically, the combination of moderate intensities, low to intermediate electron energies compared to I_p, and large system size prevent the electrons from escaping the system. Consequently, ionized areas inside a cluster or a dielectric remain overall neutral. High (solid state) plasma density in these areas leads

to strong screening, with the typical Debye radius $r_D \sim 1$ Å. The Coulomb field of the ions localized inside the ionized regions is completely screened, and the self-consistent field of the ionized region is small (see also [14] for numerical simulations using self-consistent time-dependent density functional method). As we consider 'infinite' medium, we do not consider effects related to large-amplitude collective electron oscillations [17] which may enhance local fields [14] at the poles of a cluster [18] and play a critical role in multiple ionization of small- and moderate-sized clusters [14, 17, 18].

Under such conditions enhancement of ionization (ionization ignition) will occur due to the *local deviations* from the self-consistent field. Such deviations occur at the periphery of the ionized region when a new electron–hole pair is created. Since the electrons are much lighter than the holes, laser-assisted motion of the newly created free electron will lead to its spatial separation from the positively charged hole. We assume that immediately after ionization the Coulomb field of the newly created hole at the boundary of the ionized region is not screened. This leads to local deviations from the self-consistent electric field and enhanced ionization along the boundary of the ionized region. In our model, screening can turn off the field of the newly created hole within one period of the plasma oscillations, quenching the enhancement of the ionization rate.

For numerical simulations, we model the medium as a two-dimensional $N \times N$ lattice, with N taking the values $N = 100$, $N = 200$, $N = 300$ and $N = 400$. Expansion of the ionized regions is modelled by the stochastic finite-difference equation

$$\Delta w_{i,k} = \Gamma K_{i,k} p_{i,k} \Delta t. \tag{2}$$

Here $\Delta w_{i,k}$ is the ionization probability of the site with indices i, k during the time-step Δt, Γ is the bare multiphoton (or tunnelling) ionization rate not enhanced by any local fields and $K_{i,k}$ is the enhancement coefficient determined by the presence of holes at the adjacent sites. In standard models of the breakdown of dielectrics, multiphoton ionization is only included via the bare rate Γ, and any modification due to local fields is neglected. The factor $p_{i,k}$ takes only two values, 0 or 1: $p_{i,k} = 1$ means that the site is neutral at the beginning of this time step, and $p_{i,k} = 0$ means that it is ionized. At the end of every time step, a random number $r_{i,k}$ between 0 and 1 is generated for each site, and $\Delta w_{i,k}$ is compared to $r_{i,k}$. The site is deemed ionized and $p_{i,k} = 0$ if $\Delta w_{i,k} > r_{i,k}$, while for $\Delta w_{i,k} < r_{i,k}$ the site remains neutral with $p_{i,k} = 1$. If the site is ionized, it enhances the ionization rate for adjacent sites $i' = i \pm 1, k' = k \pm 1$. Recombination is not included, since the timescales of interest here are very short, few to few tens of femtoseconds.

Multiple ionization is of course possible, but we assume that it would occur after single ionization. By the time secondary ionization would happen, the ionized region would have expanded to swallow the site of interest and screen its field. Therefore, in this model multiple ionization has no influence on the expansion dynamics of the ionized regions.

Expansion of ionized regions is determined by the time-dependent dynamics of $K_{i,k}$. If there are no adjacent holes, or if they are screened, $K_{i,k} = 1$. As discussed above, we assume that enhancement is only due to newly created holes at the periphery of ionized regions. If the site (i, k) is ionized at the end of the time-step Δt, its Coulomb field will be used to find the enhancement coefficients $K_{i',k'}$ for adjacent sites (i', k') *outside the ionized region*. This $K_{i',k'}$ will be used to calculate ionization probability of the site (i', k') during the next time step.

To find $K_{i,k}$, we first consider enhancement of the ionization rate induced in an isolated atom by the presence of a constant electric field of a hole. We begin with approximate analytical treatment which goes beyond simple tunnelling formula equation (1) and is applicable at intermediate intensities and the multiphoton regime of the Keldysh parameter $\gamma > 1$. The

validity of the analytical expressions is checked by comparing to numerical simulations. We then proceed to the numerical simulations of the overall dynamics.

In analytical calculations of ionization rates in the presence of the laser field and the static field, we do not use the original Keldysh exponent for cycle-averaged rates [16]. Instead, we follow the prescription advocated in [19]. Firstly, we obtain the main exponential dependence of instantaneous ionization rate. Secondly, the pre-exponential factor is restored by taking the limit of $\gamma \ll 1$, where this factor is accurately known.

The total electric field acting upon an atom at the lattice site is $\mathbf{E}(t) = \mathbf{E} \cos \omega t + \mathbf{E}_h$, and the corresponding vector potential is $\mathbf{A}(t) = -\frac{\mathbf{E}}{\omega} \sin \omega t - \mathbf{E}_h t$. Population of the continuum states at an instant t is

$$W(t) = \int d^3 v |a_\mathbf{v}(t)|^2 \tag{3}$$

where $a_\mathbf{v}(t)$ is the probability amplitude of populating the field-free continuum state labelled by the velocity $|\mathbf{v}\rangle$:

$$a_\mathbf{v}(t) \sim -i \int_{-\infty}^t dt' V_{vc}(t') \exp(-i S_\mathbf{v}(t, t')) \tag{4}$$

where V_{vc} is the transition dipole matrix element between the valence and the conduction bands induced by the total field, $V_{vc}(t') \propto \mathbf{r}_{vc} \mathbf{E}_{tot}(t')$, and

$$S_\mathbf{v}(t, t') = I_p(t - t') + \frac{1}{2} \int_{t'}^t dt'' [\mathbf{v} - \mathbf{A}(t) + \mathbf{A}(t'')]^2 \tag{5}$$

is the action integral, with I_p the ionization potential of an atom in a cluster or a band gap energy in a dielectric. The latest expression is analogous to the standard strong-field approximation (SFA) of atomic physics (see, for example, review by [20]).

The integral over t' for the amplitude $a_\mathbf{v}(t)$ is calculated using the saddle point method. The saddle points $t'(t)$ are given by the equation

$$\frac{1}{2}[\mathbf{v} - \mathbf{A}(t) + \mathbf{A}(t')]^2 + I_p = 0. \tag{6}$$

Due to the periodicity of the laser field, for any moment of observation t, there are many saddle points t'_n: one per laser cycle. They correspond to contributions into the total amplitude from repeated ionization events at every laser cycle. For the saddle point closest to t, denoted as t'_0, $\text{Re}(t'_0) \approx t$. Other t'_n are separated from t'_0 by the integer number of cycles, $t'_n = t'_0 - 2\pi n$, integer $n \geqslant 1$. The imaginary part of action is the same for all of them, and hence they all yield the same exponential dependence for the ionization probability.

Instantaneous ionization rate is given by the latest addition to the continuum, which corresponds to the contribution of the single saddle point t'_0 with $\text{Re}(t'_0) \approx t$. Contributions of the saddle points t'_n, $n \geqslant 1$, describe population created in the continuum one or more laser cycles ago; the corresponding action integrals contain contributions from the free electron motion in the continuum. When the electron just appears in the continuum, its instantaneous velocity $\mathbf{v}$ is small. This allows one to drop $\mathbf{v}$ from the saddle point equation [16, 19], which becomes

$$\frac{1}{2}[\mathbf{A}(t'_0) - \mathbf{A}(t)]^2 + I_p = 0. \tag{7}$$

Although this equation cannot be solved analytically, its numerical solution is trivial. Once it is found, the exponential dependence in the transition amplitude $a_{v=0}(t)$ is given by the imaginary part of the corresponding action integral and the rate is proportional to that exponent squared,

$$\Gamma \sim \exp(-2 \operatorname{Im} S_{\mathbf{v}=0}(t, t'_0)). \tag{8}$$

Normalizing this result to the case of $E_h = 0$ gives the enhancement coefficient, which is correct to within the ratio of pre-exponential factors. The pre-exponential dependence is
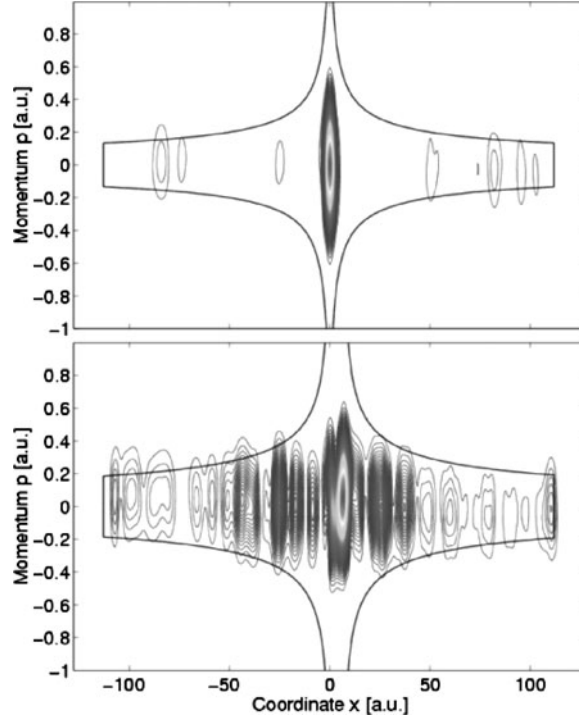
Figure 1. Husimi electron distribution around an argon (Ar) atom (top) and an Ar + Ar$^+$ ion system (bottom). Laser intensity $I = 1 \times 10^{14}$ W cm^{-2}. The solid line represents the zero-energy boundary, outside of which the parts of electron distribution can be considered ionized.

restored as described in [19]. Since ionization occurs mostly near the peaks of the instantaneous field, the enhanced cycle-averaged rate is obtained by calculating the enhancement coefficient for $\cos \omega t = 1$ and once again normalizing the answer to that for $E_h = 0$.

We now compare these analytical results with the numerical calculations of the enhancement coefficient. The numerical model is a one-dimensional grid bounded with absorbing regions, with the atomic site at its centre modelled by a soft-core (Rochester) potential [21] and the ground state electron wave packet. The ground state energies (equivalent to the band gap energy in our model) are obtained by altering the soft-core parameter ϵ within the atomic potential V

$$V = -\frac{1}{\sqrt{x^2 + \epsilon}} \tag{9}$$

where x is the position coordinate. The numerical simulations involve solving the time-dependent Schrödinger equation using the split-operator method [22]. The influence of the ion (hole) is incorporated via the addition of a second potential, centred a distance D from the atom site, either as another soft-core potential or as a homogeneous electric field E_h used in the analytical solution.

Figure 1 depicts the phase space distribution of the electron wavefunction at the end of laser pulse of duration τ, for single argon atom, as compared to the argon atom + ion system (we consider an argon cluster with the typical distance between atoms $D = 7$ au throughout the paper). The distribution is a Husimi function, or coarse-grained Wigner representation defined by [23] $H(p, x, \tau) \propto |\langle \phi_{p,x} | \psi(\tau) \rangle|^2$, where p, x are the canonical momentum and
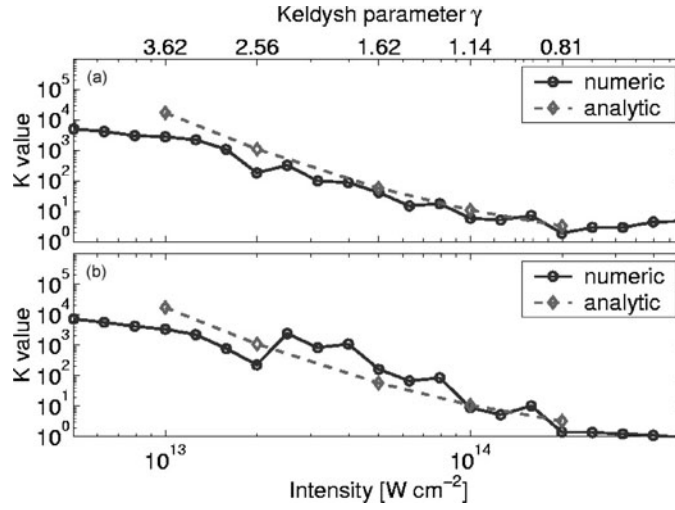
Figure 2. K values given by numerical simulations in relation to the SFA theory for a trapezoidal 1-20-1 pulse ($\lambda = 800$ nm) for argon cluster. Top plot gives comparison where, numerically, the effective field produced by the ion is a homogeneous DC field. Bottom plot has the ion field modelled by the soft-core potential.

coordinate values, respectively; $\phi_{p,x}$ is any standard coherent state, such as a minimum dispersion Gaussian wave packet, and $|\psi(\tau)\rangle$ is the final electronic state. The solid line is the zero-energy boundary, which is truncated at high x values due to the absorbing boundary conditions. By calculating the proportion of the distribution lying within the zero-energy boundary, one can find the norm of the electronic state which remains bound. It is clear that there is significant ionization enhancement due to the presence of the ion site.

To quantify the effect due to the proximity of the hole, we define the factor K to be Γ_1/Γ_0, where Γ_1 and Γ_0 are the ionization rates with and without the presence of the ion, respectively. Γ is calculated as the rate of change of the time-dependent norm of the electronic state, obtained by fitting to an exponential rate equation: $|\psi(\tau)|^2 = \exp(-\Gamma\tau)$. The final norm is determined by projecting out the ground state $|g\rangle$ for a single atom, and the ground state plus first excited state $|e\rangle$ for the atom + ion system, from the final electronic state. These states belong to the valence band of the two-site system. The norms determined this way are in agreement with those determined via inspection of the Husimi distribution method described above.

Figure 2 compares analytical results with the numerical calculations of the enhancement coefficient K in the case of argon. Analytical theory produces a continuous enhancement curve (rather than discrete data points), from which we have highlighted 5 points for comparison with numerics. When the hole is treated as a homogeneous electric field (figure 2(a)), the numerical and analytical results are in good quantitative agreement even at low intensities where $\gamma \approx 4$, and ionization is in the multiphoton regime. What is the origin of this surprising agreement? Firstly, the effect of the ionic core on the total ionization rate is partially included in the analytical model by normalizing the pre-exponential factor to obtain correct rates in the tunnelling limit $\gamma \ll 1$. This takes care of correcting the shape of the potential barrier for tunnelling. Secondly, even for $\gamma > 1$ ionization mainly occurs via non-adiabatic tunnelling [19], i.e. via the motion in the classically forbidden under-the-barrier region—even though at $\gamma > 1$ this barrier no longer appears static to the tunnelling electron. The main flaw of
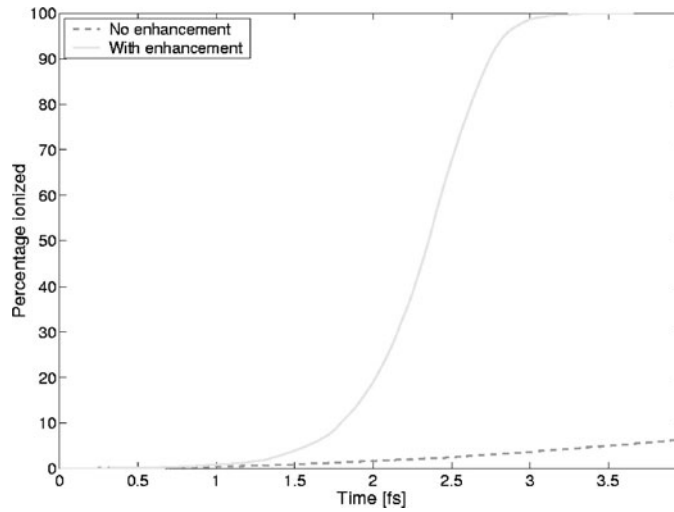
Figure 3. The percentage of argon cluster surface area ionized, plotted as a function of time. The dashed line corresponds to the case for no enhancement ($K_{i,k} = 1$), whereas the solid line includes enhancement. Laser parameters are $I = 5 \times 10^{13}$ W cm^{-2} and $\lambda = 800$ nm.

the Keldysh-type model used here is that it completely ignores wavefunction dynamics in the classically allowed region, i.e. possible excitations inside the potential well. Fortunately, for small photon energies and systems with large energy gap to the first-excited states, such 'inside-well' excitation is weak and non-adiabatic tunnelling dominates even at moderately large values of γ. The situation would change completely if the excited states were close to the ground state—then 'inside-well' excitation would play a dominant role and the Keldysh-type approach would fail. Indeed, as seen in figure 2(b), additional structures are apparent in the numerical results when the ion is described as a soft-core potential. We have verified that these structures are due to dynamics inside the double-well potential: resonances between the wells and population trapping in excited states.

Having established the validity of our analytical expressions, we can now use the enhancement coefficient to simulate the ionization dynamics in the cluster or a dielectric. We use analytical expressions which are valid for any geometry of holes and/or polarization of the laser field, to obtain the enhancement coefficients and we use results of numerical simulations for the basic ionization rate Γ. In the present paper we are not concerned with the kinetics of non-equilibrium plasmas. The build-up of screening in a plasma takes place in approximately one plasma period (see, for example, [24], previous predictions [25] and references therein). We require that the timescale for the development of a forest fire $\tau_f < 2\pi/\omega_p$, where ω_p is the plasma frequency. Therefore, we pick an example where the τ_f is very small. We consider an argon cluster in a laser field with intensity $I = 5 \times 10^{13}$ W cm^{-2}. Our calculations confirm that $\tau_f < 2\pi/\omega_p$ until the fractional ionization reaches 50%.

Figure 3 shows the percentage of ionized sites in an argon cluster as a function of time, with and without enhancement for the 100×100 lattice. For this model calculation the field is turned on instantaneously. We use the enhanced ionization rates averaged over one quarter of the laser cycle. In the absence of enhancement complete ionization occurs in 40 fs, while with enhancement ionization is complete within only 3.5 fs. Since our calculation uses rates averaged over one-quarter of laser cycle, for such short times it is likely to overestimate the efficiency with which ionized regions expand in the medium. Nevertheless, the most important qualitative result—the dramatic speedup of ionization—is unquestionable.
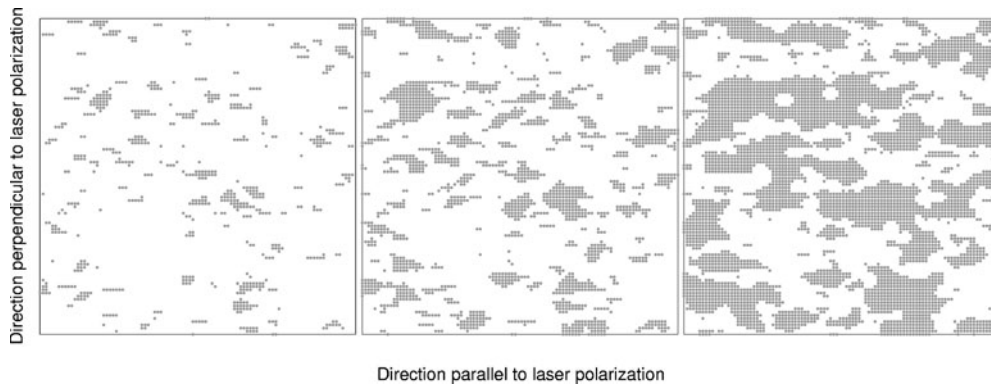
Figure 4. Two-dimensional forest fire simulation of Ar cluster surface, with laser parameters as in figure 3. Plots from left to right correspond to times at which ionized regions make up 10%, 25% and 50% of the lattice area.
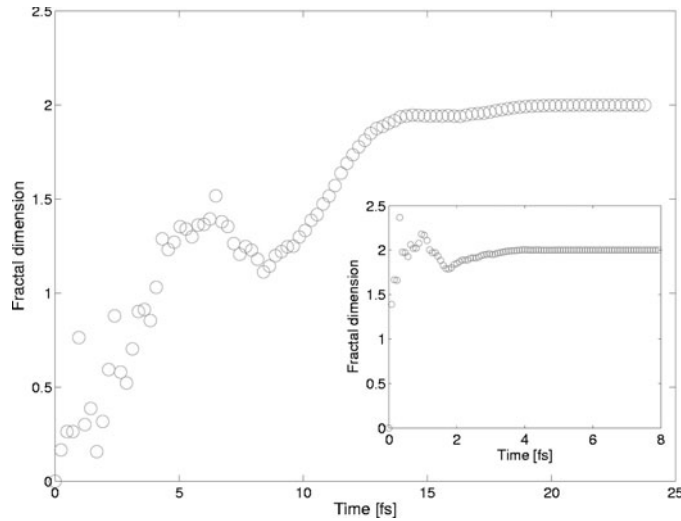

Figure 5. Dimensionality of the area of ionized regions plotted against time for $I = 2 \times 10^{13}$ W cm^{-2} and $I = 5 \times 10^{13}$ W cm^{-2} (inset). For every factor increase in lattice length ($N \rightarrow \alpha N$), the lattice area increases as α^2, while the number of ionized sites at any given time increases as α^F, where F is the fractal dimension. The noise within the first 7 fs (1 fs for the inset) is due to statistically insignificant number of ionized sites.

Figure 4 shows the expansion of multiphoton forest fire on the square $N \times N$ lattice for $N = 100$, at three stages during the ionization process corresponding to 10%, 25% and 50% ionization. The most important feature clearly visible in figure 4 is the presence of nano-scale islands of fully ionized plasma. These islands expand rapidly, mostly in the direction of polarization of the laser field, which in this figure is horizontal.

To investigate the geometrical properties of the nano-structures dynamically created inside the medium, we have repeated the calculations for an increasing size of the $N \times N$ lattice, enlarging N to $N = 200$, then $N = 300$ and then $N = 400$. We then determined how the ionized fraction, measured at the same instants of time, changes with N. The result is shown in figure 5 for $I = 2 \times 10^{13}$ W cm^{-2} and $I = 5 \times 10^{13}$ W cm^{-2} (inset).

Initially, the number of ionized sites is too small to have the good statistics necessary to determine the dimensionality of the damaged (ionized) area. As the number of ionized sites becomes statistically significant, two tendencies determine the growth of the damaged area. Firstly, there is ionization of sites which are not in the vicinity of any ionized island. The number of these sites is proportional to the total number of lattice sites and hence grows quadratically with N. Secondly, already created holes enhance the growth predominantly along the laser polarization and hence the area of these islands grows linearly with N at early times. Competition between these two tendencies determines early dynamics, with the fractal dimension initially decreasing as the linear growth of islands begins to dominate the total damaged area. This decrease is, however, limited and is replaced by the growth of the fractal dimension after the minimum. This growth reflects the fact that islands grow not only parallel to laser polarization, but also at an angle to it. Finally, the fractal dimension approaches two when the islands start to merge. Between these two limits, the dimension of the nano-islands is fractal. The appearance of fractals in forest-fire type dynamics is not unusual [26]. However, they are usually associated with steady-state structures that arise when there is a recovery mechanism for 'burned' areas. In our case screening of ionized sites could, in principle, have been considered as somewhat analogous to such a recovery mechanism. However, we do not count screening as recombination of ionized sites and do not exclude screened sites from the ionized structures. This is why the fractal structures that we observed are not steady state but rather arise and disappear dynamically as islands of nano-plasma merge together.

Thus, our simulations show highly inhomogeneous ionization and therefore inhomogeneous deposition of laser energy inside the dielectric. Nano-droplets of plasma have a broad variety of sizes and geometries, from sub-nanometer to few tens of nanometers. This means that interaction of the laser pulse with the dielectric becomes similar to laser interaction with nanostructured composite materials, where metallic nano-particles are inserted into the dielectric host—only here these nano-particles are created by the same laser field. Interaction of infrared laser radiation with nano-structured metal–dielectric composites gives rise to a variety of important effects [27, 28]. The most notable for us is the excitation of surface plasmons in the nano-particles and associated with it the giant enhancements of local electric fields at sub-wavelength scale [27, 28]. The fractal nature of the dynamically created nano-structures or, more generally, the broad distribution of nano-particle sizes and shapes means that the laser radiation inevitably finds a resonance with the surface plasmon frequency of appropriately sized/shaped nanoparticles. Excitation of surface plasmons and enhancements of the local fields further enhances very efficient and highly inhomogeneous deposition of the laser pulse energy into the nano-scale areas.

Thus, we suggest that the overall dynamics of ultrafast laser-induced damage at moderate intensities below the conventional breakdown threshold should develop as an interplay between at least two different mechanisms, none of which is associated with the traditional electron avalanche. First is 'seeding' of small nano-plasmas which grow like forest fires. Their growth is associated with the fluctuations of the local fields around the self-consistent field and can be quenched by fast screening of the newly created holes. Second is the excitation of surface plasmons in these particles which leads to large enhancements of the local field (similar to those occurring near any nano-sized metal tip) and further amplifies highly inhomogeneous deposition of laser energy at sub-wavelength scale. The present work has only addressed the first component of this process. Full dynamical simulations including propagation of the laser light and depletion of the laser energy will be the subject of future work.

Acknowledgments

References

[1] Taylor R S, Hnatovsky C, Sminova E, Rayner D M, Bhardwaj V R and Corkum P B 2003 *Opt. Lett.* **28** 1043
[2] Glezer E N, Milosavljevic M, Huang L, Finlay R J, Her T-H, Callan J P and Mazur E 1996 *Opt. Lett.* **21** 2023
[3] Sudrie L, Franco M, Prade B and Mysyrowicz A 2001 *Opt. Commun.* **191** 333
   Sudrie L, Couairon A, Franco M, Lamouroux B, Prade B, Tzortzakis S and Mysyrowicz A 2002 *Phys. Rev. Lett.* **89** 186601
[4] Davis K M, Miura K, Sugimoto N and Hirao K 1996 *Opt. Lett.* **21** 1729
   Miura K, Inouye H, Jianrong Q, Mitsuyu T and Hirao K 1998 *Nucl. Instrum Methods Phys. Res.* B **141** 726
[5] Homoelle D, Wielandy S and Gaeta A L 1999 *Opt. Lett.* **24** 1311
[6] Kumarappan V, Krishnamurthy M and Mathur D 2003 *Phys. Rev.* A **67** 043204
[7] Ditmire T, Tisch J W G, Springate E, Mason M B, Hay N, Smith R A, Marangos J P and Hutchinson M H R 1997 *Nature* **386** 54
   Ditmire T, Tisch J W G, Springate E, Mason M B, Hay N, Marangos J P and Hutchinson M H R 1997 *Phys. Rev. Lett.* **78** 2732
[8] Lezius M, Dobosz S, Norman D and Schmidt M 1997 *J. Phys. B: At. Mol. Opt. Phys.* **30** L251
   Lezius M, Dobosz S, Norman D and Schmidt M 1998 *Phys. Rev. Lett.* **80** 261
   Springate E, Hay N, Tisch J W G, Mason M B, Ditmire T, Hutchinson M H R and Marangos J P 2000 *Phys. Rev.* A **61** 063201
[9] Siedeman T, Ivanov M Yu and Corkum P B 1995 *Phys. Rev. Lett.* **75** 2819
   Chelkovski S and Bandrauk A D 1995 *J. Phys. B: At. Mol. Opt. Phys.* **28** L723
   Siedeman T, Ivanov M Yu and Corkum P B 1996 *Chem. Phys. Lett.* **252** 181
   Gibson G N, Dunne G and Bergquist K J 1998 *Phys. Rev. Lett.* **81** 2663
[10] Rose-Petruck C, Schafer K J, Wilson K R and Barty C P J 1997 *Phys. Rev.* A **55** 1182
   Hu S X and Xu Z Z 1997 *Phys. Rev.* A **56** 3916
[11] Véniard V, Taïeb R and Maquet A 1999 *Phys. Rev.* A **60** 3952
   Véniard V, Taïeb R and Maquet A 2001 *Phys. Rev.* A **65** 013202
[12] Last I and Jortner J 2000 *Phys. Rev.* A **62** 013201
[13] Siedschlag C and Rost J M 2002 *Phys. Rev. Lett.* **89** 173401
   Siedschlag C and Rost J M 2003 *Phys. Rev.* A **67** 013404
[14] Bauer D and Macchi A 2003 *Phys. Rev.* A **68** 033201
[15] Yudin G L, Gaier L N, Lein M, Knight P L, Corkum P B and Ivanov M Yu 2004 *Laser Phys.* **14** 51
[16] Keldysh L V 1964 *Zh. Eksp. Teor. Fiz.* **47** 1945
   Keldysh L V 1965 *Sov. Phys.—JETP* **20** 1307 (Engl. Transl.)
[17] Saalmann U and Rost J M 2003 *Phys. Rev. Lett.* **91** 223401
[18] Jungreuthmayer C and Brabec T submitted
[19] Yudin G L and Ivanov M Yu 2001 *Phys. Rev.* A **64** 013409
[20] Protopapas M, Keitel C H and Knight P L 1997 *Rep. Prog. Phys.* **60** 389
[21] Javanainen J, Eberly J H and Su Q 1988 *Phys. Rev.* A **38** 3430
[22] Feit M D, Fleck J A and Steiger A 1982 *J. Comput. Phys* **47** 412
[23] Życzkowski K 1987 *Phys. Rev.* A **35** 3456
[24] Huber R, Tauser F, Brodschelm A, Bichler M, Abstreiter G and Leitenstorfer A 2001 *Nature* **414** 286
   Leitenstorfer A, Huber R, Tauser F, Brodschelm A, Bichler M and Abstreiter G 2002 *Physica* B **414** 248

[25] Sayed K El, Schuster S, Haug H, Herzel F and Henneberger K 1994 *Phys. Rev.* B **49** 7337
      Kwong N-H and Bonitz M 2000 *Phys. Rev. Lett.* **84** 1768
      Vu Q T and Haug 2000 *Phys. Rev.* B **62** 7179
[26] Drossel B and Schwabl F 1992 *Phys. Rev. Lett.* **69** 1629
      Fröjdh P and den Nijs M 1997 *Phys. Rev. Lett.* **78** 1850
[27] Stockman M I, Pandey L N, Muratov L S and George T F 1994 *Phys. Rev. Lett.* **72** 2486
      Stockman M I, Pandey L N and George T F 1996 *Phys. Rev.* B **53** 2183
      Grésillon S, Aigouy L, Boccara A C and Rivoal J C 1999 *Phys. Rev. Lett.* **82** 4520
      Stockman M I 2000 *Phys. Rev.* B **65** 10494
      Stockman M I 2000 *Phys. Rev. Lett.* **84** 1011
      Bergman D J and Stockman M I 2003 *Phys. Rev. Lett.* **90** 027402
[28] Shalaev V M 2000 *Nonlinear Optics of Random Media: Fractal Composites and Metal–Dielectric Films
      (Springer Tracts in Modern Physics* vol 158*)* (Berlin: Springer)
      Shalaev V M (ed) 2002 *Optical Properties of Random Nanostructures (Topics in Applied Physics* vol 82*)* (Berlin:
      Springer)
      Genov D, Sarychev A K and Shalaev V M 2003 *Phys. Rev.* E **67** 056611